Bio-sourced Poly L-Lactide-Flax Composites with Close To Maximum Stiffness at Low Fiber Content through Two-Stage Annealing

Rajendar Nutenki[a], Pascal Van Velthem[a], Martial Kuete[a], Matthieu Lezaak[b],Vincent Destoop[b], Wael Ballout[a], Thomas Pardoen[b], Christian Bailly[a]*

[a] *Institute of Condensed Matter and Nanosciences - Bio & Soft Matter (IMCN/BSMA), UCLouvain, 1348, Louvain-la-Neuve, Belgium*

[b] *Institute of Mechanics, Materials and Civil Engineering, UCLouvain, 2 Place Sainte Barbe, 1348 Louvain-la-Neuve, Belgium*

** E-mail : christian.bailly@uclouvain.be*

Abstract

Poly L-lactide (PLLA) composites with short flax fibers (from 0 to 10 wt/wt%) with close to maximum theoretical stiffness are prepared by melt-compounding and injection-molding followed by a two-step isothermal crystallization protocol that fully separates the nucleation and growth stages (Tammann). The use of ultrafast scanning chip calorimetry for thermal characterization avoids the complicating issues of crystal reorganization during the cooling and heating steps between the isothermal stages. Flax fibers are very efficient and selective nucleating agents of PLLA favoring the ordered α form. The resulting morphology exhibits trans-crystallization on the fibers surface, predominantly at fiber defects, with a clear reduction of crystal size and a very strong fiber matrix cohesion. Efficient nucleation further leads to a large reduction of the overall crystallization time. Avrami analysis evidences a reduction of crystal growth dimensionality, consistent with both optical and scanning electron microscopy. The high modulus of the composites is unambiguously related to the strong orientation of the fibers in the tensile direction, to their high aspect ratio and to the excellent matrix-fibers cohesion. On the other hand, the tensile strength and hardness appear isotropic within experimental uncertainty and are unfavorably influenced by the presence of the fibers and by the two-stage annealing.

Key words

PLLA, Flax, Bio-composites, Fast Scanning Chip Calorimetry, Trans-crystallization, Tammann, Voigt Model |

1. Introduction

Increasing environmental consciousness and growing worries about global warming have led in recent years to a renewed interest in the use of carbon neutral ligno-cellulosic fibers as reinforcers and fillers in polymer composites. [1-3] Flax fibers stand out because of their low density, remarkable aspect ratio, which contributes to a high surface area, and high cellulose content, leading to high tensile strength as well as modulus. Flax fibers reinforced polymer composites have already found their use in a wide range of non-structural applications [4, 5] and are attractive candidates for structural polymer reinforcement. Natural fibers, including flax, are further well proven nucleating agents of bio based polymers, including poly L-lactic acid (PLLA), which is a prime candidate as replacement of oil-based polymers for carbon neutral applications, owing to its adjustable mechanical properties and relatively low-cost of production.[6] However, neat PLLA crystallizes very slowly because of a relatively rigid chain [7-9] and specific processing conditions, including lengthy annealing, are needed to ensure optimal mechanical properties. The mechanical properties of PLLA-based artifacts, like those of all crystalline polymers, are controlled by the characteristics of the crystalline phase, including the crystalline fraction, the crystalline form, and the crystalline morphology. [10-14] Moreover, the presence of a specific crystalline form can affect the adhesion between the polymer and a reinforcing fiber, either positively or negatively with corresponding consequences on the mechanical properties. [15] Recent studies have shown that flax fibers are able to enhance and speed up crystal nucleation of PLLA under suitable conditions, resulting in higher crystallinity and shorter crystallization times.[16, 17] Moreover, the tensile modulus of crystalline polymers, including PLLA, is not solely controlled by the crystalline fraction but also by any hetero-phase nucleating agent since both impact the crystalline and amorphous regions, which in turn affects the modulus.[18, 19]

PLLA exhibits a complex polymorphism that depends on temperature, mechanical deformation and epitaxy. [20-22] So far, four different crystal forms (named α -, β-, γ-, and ε-forms) have been identified. Under quiescent conditions (via solution, melt, or cold crystallization), PLLA crystallizes in a dominant α' form below 100°C, which is metastable and disordered, while the ordered α phase prevails above 120°C. [23–25] A coexistence and progressive transition from dominance of one to the other is observed in the intermediate temperature range between 100 and 120°C. [23–25] FTIR, Raman and X-ray diffraction have been used to identify this complex behavior

by selective annealing procedures, which subsequently affect the properties of PLLA and of its composites. [23-25]

The newly developed experimental technique of fast scanning chip calorimetry (FDSC), the commercial version of which is known as "Flash DSC", can follow heating/cooling rates up to 5000 K/s and has become an important tool in the study of non-isothermal and isothermal crystallization of polymers. [26–28] Recently, FDSC measurements have confirmed the melting-recrystallization behavior of PLLA α′/α -crystals at elevated temperatures. [29] The ultra-fast cooling rates made possible by FDSC allow a precise control of the thermal processing conditions and offer a uniquely detailed method to study the effect of nucleating fibers on the crystallization and resulting microstructure, which can help design optimized PLLA composites. [29, 30]

Although the PLLA crystal phase and morphology have a major influence on the properties of the corresponding fiber-reinforced composites, the exact mechanism for their development in the presence of fibers is not yet fully established. The surface chemistry and topography of the fibers [31, 35] as well as the residual stresses at the fiber/matrix interface generated during cooling due to the discrepancy between the thermal expansion coefficients of the two materials [13] play a key role in the phase transformation processes. Clearly, the fibers can induce extremely effective nucleation, which hinders the development of spherulites and thus forces crystal growth to proceed only in the direction perpendicular to the fiber long axis. This peculiar morphology is referred to as a trans-crystallinity (TC) on the fiber surface and is ascribed to a high nucleating ability by the fiber. [31-35] Several detailed investigations have suggested that the development of TC can be attributed to two main causes, which are (i) fiber-induced nucleation and (ii) crystal perpendicular growth on the fiber surface.

A century ago, Tammann proposed a two-stage process to separate crystal nucleation (at T_{nuc}) from crystal growth (at T_d) stages in order to rationalize the crystallization process.[36] Tammann's method decouples the two through an "instantaneous" temperature jump from T_{nuc} *to* $T_d > T_{nuc}$. Since the work of Tammann, two-stage thermal annealing has been used to afford experimental access to the nucleation kinetics of extremely undercooled melts. The crystal nucleation rates of neat PLLA have been widely studied by this method but not of its composites. [37-39]

T_{nuc} is chosen as to strongly favor the nucleation rate i over the growth rate g, hence the overall crystallization rate is low and multiple nuclei spread (on the fiber surface) with either α'/α

dominance or coexistence depending on temperature, before the completion of a single crystal layer. [8, 26-28] On the contrary, at T_d, i must be very small compared to g, hence a single nucleus spreads over the surface before another nucleus is formed, typically resulting in the crystallization of the α form.

To the best of our knowledge, the influence of the α'/α-crystal polymorphism on the properties of PLLA-flax composites has not been studied over a broad range of time and temperature. In particular, the influence of controlled nucleation and growth leading to pure ordered α crystals and the related effect on the mechanical properties is still poorly understood.

In the present work, the effect of flax on the (interfacial) crystallization of PLLA has first been studied using the Tammann approach with the help of FDSC in order to separate the nucleation and growth stages and favor the ordered phase. Next, microscopy has been used to understand crystal growth on the fibers surface and detect trans-crystallization as well as fiber/matrix interfacial adhesion. Finally, the effect of flax on the thermomechanical properties of pure α-phase composites manufactured by melt mixing in co-rotating twin screw extruder and subsequently injection molded has been clarified. The mechanical properties have been evaluated by DMTA, tensile testing and hardness, primarily on two stage annealed specimens.

2. Experimental Section

Full experimental details on materials, processing and characterization are provided in the Supplementary Information (Section S1, in Appendix). Only a summarized version is provided below due to length constraints.

2.1. Materials

UD flax fiber fabrics (AmpliTex ® UD type 5057) were provided by Bcomp® (Fribourg, Switzerland). According to the manufacturer, these fabrics have excellent compatibility with polyesters and are suitable for extrusion and molding processes. The as-received fabrics were finely chopped into discrete fibers with 0.4-0.5 mm length. Ingeo™ PLLA (grade 2500HP) was supplied in pellets form by *Nature Works LLC*.

2.2. Processing

The chopped fibers were dried at 105°C under vacuum for 12 hours to remove moisture. In order to prevent polymer degradation by hydrolysis during extrusion, the as-received PLLA was dried overnight at 60°C under vacuum. The processing conditions recommended in the *Nature Works* technical data sheet were followed.

PLLA and PLLA/flax blends containing 1, 5 and 10% w/w respectively were compounded in a Thermo Scientific Process 11 co-rotating twin screw extruder. The compounds will be referred to as PLLA-F*x*, with *x* the weight percentage of flax fibers.

The set temperature profile of the heating zones (T_2 to T_8) ranged from 190 to 210°C from hopper to die and the screw speed was 150 rpm. The residence time in the extruder was around 1 min. The extruded composite strands were immediately quenched in cold water and pelletized. The pellets were dried for 6 hours at 60°C before injection molding.

Dried compounded pellets were injection-molded (IM) to produce dog-bone test pieces (ISO 527-2-5A mould) by using a Thermo Scientific™ HAAKE™ MiniJet Pro. Molding parameters were as follows: cylinder temperature 220°C, mould temperature 70°C, pressure 600 bar, post pressure 500 bar, both maintained for 30 seconds. Because the machine configuration only allows for sequential injection and cooling of individual moldings, the residence time in the melt reservoir ranged from about 1 to 8 min to produce 4 test specimens. We found no residence time-related drift of the properties reported in Table 1 as demonstrated by the low standard deviation values shown between square brackets below the averages.

Based on the FDSC findings (Section 3.1), a two-stage annealing treatment was applied to some injection-molded tensile bars, consisting of an isothermal nucleation step at 70°C for 360s followed by a crystal growth step at 125°C for 600s, both in an oven *in vacuo*. Further details can be found in the Supplementary Information.

2. 3. Characterization Techniques

2.3.1. Fast-scanning chip-calorimeter (FDSC)

FDSC crystallization experiments were performed in a Flash DSC 1 instrument from Mettler-Toledo connected to an intercooler and nitrogen purge gas. The calorimetric chip-sensor was conditioned three times and corrected one time prior to use according to the standard procedure. The samples were cut from extruded pellets into slivers with approximate thickness of 10 μm and weight of about 100-250 ng with the help of a sharp razor and positioned at the center of the microchip sensor. The exact weight of the samples was inferred by comparison between enthalpies measured on the FDSC and a conventional DSC for the same pellet. The crystallinity of the samples was calculated based on a pure crystal melting enthalpy of 107 J/g for the α' and 143 J/g for the α forms respectively.[25] It was further corrected for the polymer content in composite samples by dividing the measured value by the polymer weight fraction of the sample. Further details are provided in Supplementary Information (Section S1.3.1).

2.3.2. Dynamic mechanical thermal analysis (DMTA)

The viscoelastic properties of the two-stage annealed composites were analyzed in tensile mode on a DMA/SDTA861e DMTA by Mettler Toledo, equipped with a 40N load cell. At least two test specimens were obtained by cutting moldings to the desired average size (L*W*H = 9*4*2.5 mm) and used after drying overnight at 60°C in an oven *in vacuo*. The heating scan was performed at 3°C/min from 20 to 150°C, at a constant frequency of 1 Hz, maximum force of 2N and maximum displacement of 1μm, all well within the linear range.

2.3.3. Tensile Tests

Tensile tests were carried out on as-molded and two-stage annealed composites previously dried overnight at 60°C in an oven *in vacuo*. The samples were tested at room temperature at a relative humidity of 50% on a Zwick Roell test machine at a crosshead speed of 5mm/min. At least five specimens of each composite were tested and the average values are reported.

2.3.4. Microhardness Tests

Vickers microhardness tests were performed with the help of an EMCO-test DuraScan G5 indenter machine equipped with a Vickers diamond tip on double-annealed test specimens at 1 and

10kg indentation force after 10s dwell time. The investigated surfaces were located at the very center of the sample. Both perpendicular and parallel sections to the loading direction were prepared and tested in order to determine the influence of fibers orientation and/or anisotropy.

2.3.5. Polarized optical microscopy (POM)

PLLA and composites were observed by POM on a AX70 microscope from Olympus coupled with a Mettler Toledo FP90 hot-stage. The neat PLLA and PLLA/flax composites were placed between two glass slides. Samples were first heated from 20 to 220°C at 20°C/min and held at that temperature for 1min to allow complete melting, then cooled as fast as possible to 70°C for 6 min in order to avoid any crystallization. Finally, the samples were heated to 125°C during 10min for the crystal growth stage.

2.3.6. Scanning electron microscopy (SEM)

The fracture surfaces of the tensile specimens were analyzed by SEM on a JEOL 7600F instrument. A thin layer of gold (around 10 nm) was coated by sputtering on the surface of the composite specimens prior to observations.

3. Results and discussion

3.1. Fast-scanning chip-calorimeter (FDSC)

We first study by FDSC the isothermal crystallization of neat PLLA and the composites described in the Experimental section. The representativity of the tiny FDSC samples for the thermal behavior of the macroscopic composites is addressed in detail in the Supplementary Information (Section S1.3.1). This analysis has led us exclude the PLLA-F1 sample from the FDSC results but has confirmed the representativity of PLLA-F5 and -F10. The potential influence of matrix degradation by hydrolysis during processing, annealing or FDSC measurements on the crystallization behavior of the composites owing to the hygroscopic nature of the fibers is also addressed in the Supplementary Information (Section S2 in Appendix). The conclusion is that the issue is minor and does not significantly impact the findings. The FDSC temperature programs are shown in Figure 1 and are chosen to fully separate the nucleation and crystal growth stages. Between the isothermal steps, fast cooling and heating ramps of ±1000 K s^{-1} are imposed. It has been demonstrated that

PLLA crystals and homogeneous nuclei are not formed or reorganized at this high rate. [26, 29] The T_g of PLLA is around 60 to 65°C. Considering that the flax fibers can act as strong nucleators [29, 30], the nucleation temperature T_{nuc} is chosen just above, i.e. 70°C with 360s annealing time. The samples have previously been melted at 220°C for 1s, a temperature well above the equilibrium melting temperature of 207°C in order to avoid self-seeding [29], followed by quenching down to T_{nuc} (70°C) at 1000 K s^{-1}. After the nucleation period, the samples are subjected to two protocols for the growth stage in order clarify the influence of flax on the growth rate, trans-crystallization and crystalline form at T_d. [30] In the first protocol, T_d is varied from 80 to 140°C and the crystallization time kept constant at 600s (Figure 1a), while in the second one, T_d is kept constant at 125°C but the time is varied from 1 to 2000s (Figure 1b). After crystallization, the samples are cooled to 25°C and next melted at 1000 K s^{-1} to determine the crystallinity and melting point.

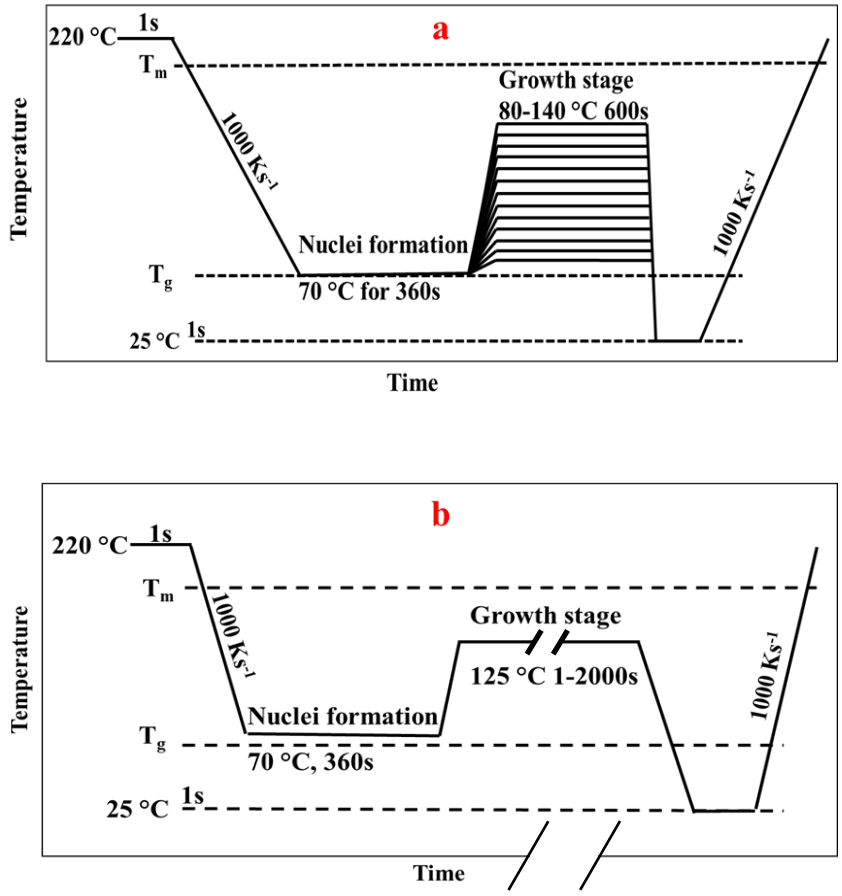

Figure 1

FDSC protocols 1 (a) and 2 (b); see text for details.

3.1.1. Effect of flax fibers on melting and crystallization kinetics at various isothermal crystal growth temperatures

Figure 2 shows the crystallization rates of all the samples at increasing T_d after completion of the nucleation step (first protocol). Visual inspection immediately shows that the fastest rates are located in the middle of the T_d range and that the composites crystallize faster than neat PLLA.

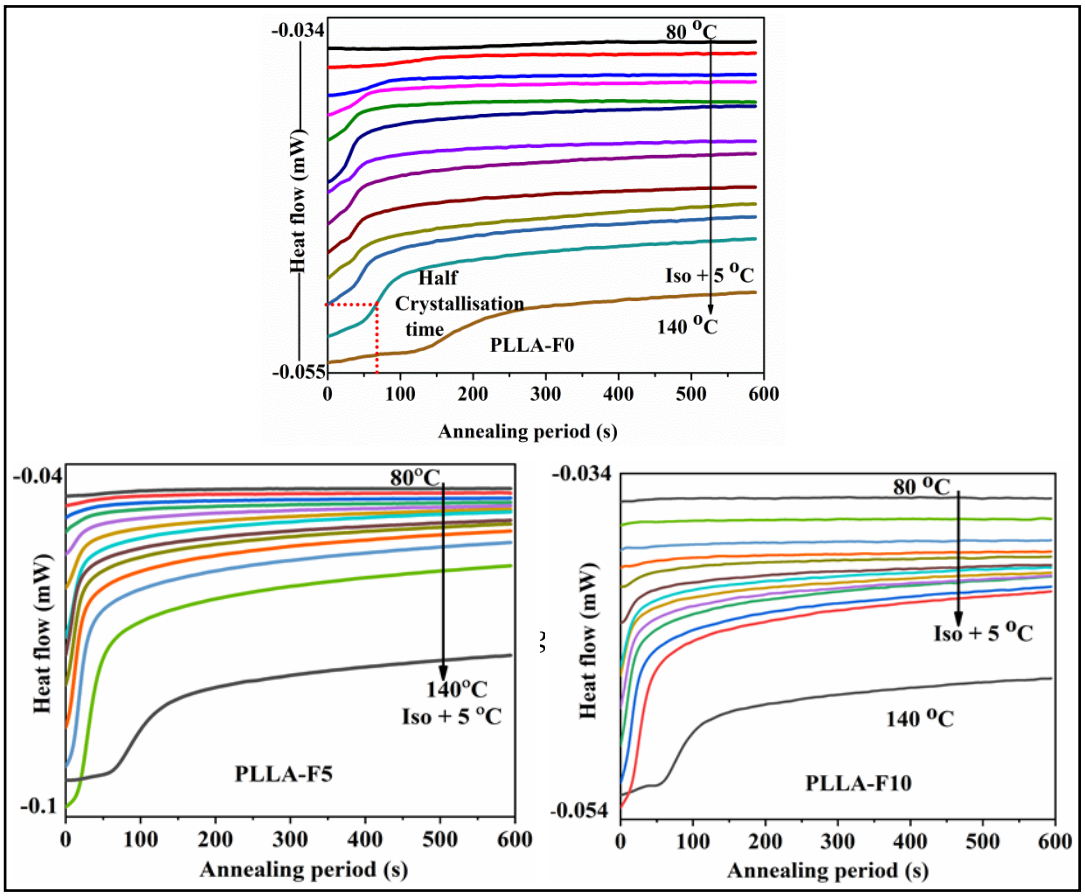

Figure 2

Effect of flax content on the crystallization rate of PLLA as a function of isothermal crystal growth temperatures from 80 to 140°C for 600s, after isothermal crystal nucleation at 70°C for 360s.

Figure 3 shows the corresponding melting curves of neat PLLA and PLLA-F10 after crystallization under the same protocol (scan rate = 1000 K s^{-1}). The melting peak temperatures strongly increase with increasing crystallization temperatures, as expected. No double melting peaks are observed as would be the case in a conventional DSC, due to the complete absence of recrystallization during the heating scan.

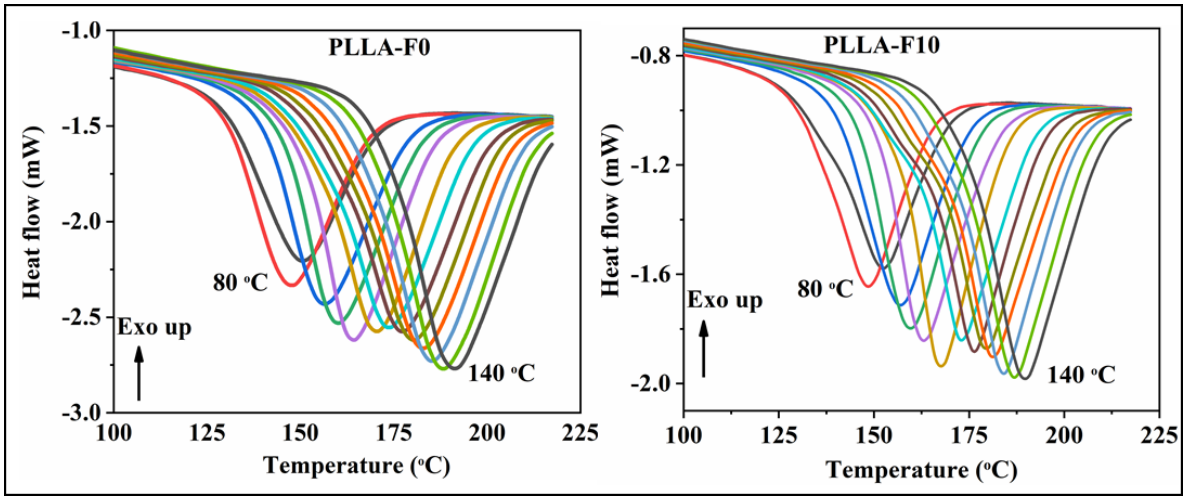

Figure 3

Effect of flax content on the melting peaks of PLLA-F0 and PLLA-F10 after isothermal crystal nucleation at 70°C for 360s followed by isothermal crystal growth from 80 to 140°C for 600s.

The vertical midpoints (i.e. half crystallization times) of the sigmoidal crystallization curves shown in Figure 2 are converted to crystallization rates in Figure 4 by taking the inverse. The observed rates correspond to a pure growth stage because of the thermal protocol selected. However, these macroscopic rates cannot be directly converted to microscopic crystal growth rates because the nucleation density and crystal shapes are a priori different from sample to sample. An Avrami analysis of selected crystallization rate curves has been performed to shed light on the growth dimensionality of the crystals: see Section 3.2.

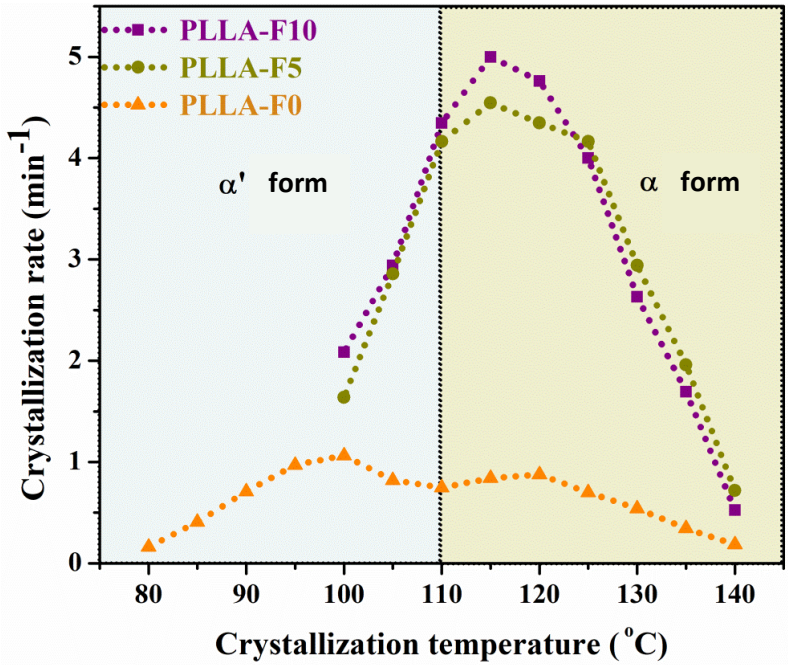

Figure 4

Effect of flax content on the crystallization rate as a function of isothermal crystal growth temperatures from 80 to 140°C, according to protocol 1. The vertical line shows the approximate temperature for the change from α' form to α form dominance.

As shown in Figure 4, the temperature dependence of the growth rates of neat PLLA is strongly bimodal with regions corresponding to α' crystals (disordered phase) from 80 to 100°C and α crystals (ordered phase) from 115 to 140°C. In the intermediate zone from 100 to 115°C, the two phases presumably coexist. These findings are consistent with earlier reports. [10-12] The α' peak of neat PLLA has the higher amplitude, with a temperature at maximum of 100°C while the α maximum is located at 120°C. When the flax content is increased to 5 wt% (PLLA-F5) the rate goes up, the bimodality disappears and the α form becomes dominant. The maximum crystallization velocity of neat PLLA is less than 1 min^{-1}. It increases to 4.5 min^{-1} for PLLA-F5 and 5.2 min^{-1} for PLLA-F10. These results indicate that flax fibers are not only acting as strong nucleation enhancers of PLLA but also selectively favor the α phase. Moreover, the main nucleation rate enhancement is already achieved at 5% flax with only minor (if any) further improvement at 10%

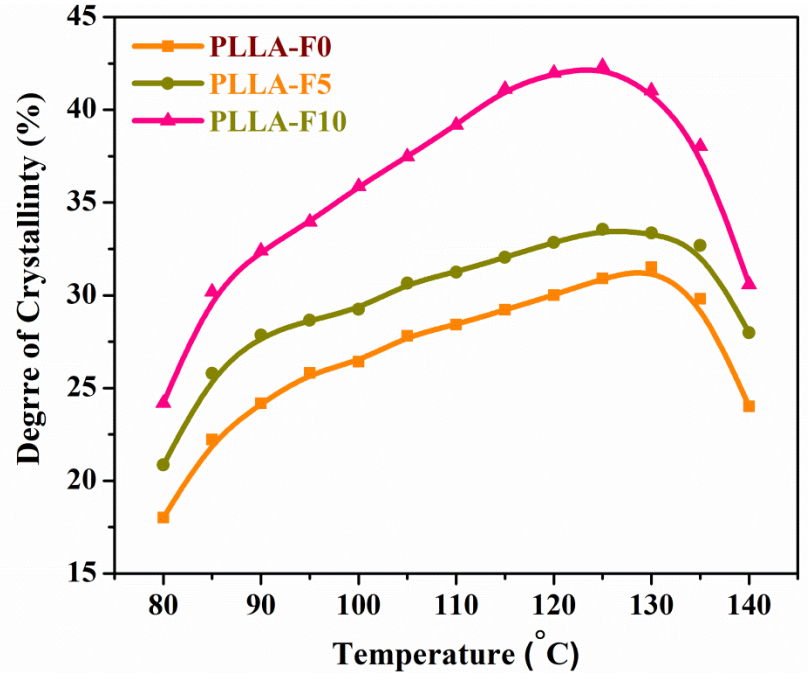

Figure 5

Influence of flax content on crystallinity after isothermal crystal nucleation at 70°C for 360s followed by isothermal crystal growth stage at temperatures from 80 to 140°C for 600s.

The degree of crystallinity of neat PLLA, PLLA-F5 and PLLA-F10 have been calculated as explained in Section 2.3.1 from the corresponding melting enthalpies obtained by integrating the melting peaks reported in Figure 3 and are shown in Figure 5 as a function of T_d. The extreme scanning rates achieved by the FDSC ensure that the pre-exiting crystals do not reorganize during heating. The degree of crystallinity of the composites is significantly higher than that of neat PLLA at all crystal growth temperatures. Moreover, the shape of the curve is different: crystallinity progressively increases from T_d = 80°C up to =130°C in the case of neat PLLA (owing to the dominance of chain mobility on crystallization rates far from the melting point) whereas PLLA-F5 and -F10 show a maximum degree of crystallinity at T_d =125°C, which reflects the downward shift of the maximum rate temperature as flax content is increased. Beyond the optimum T_d, the crystallinity drops precipitously for all samples as the thermodynamic driving force for crystallization is strongly reduced, negatively affecting the growth rates. In the next paragraph, we explore the crystallization behavior of the composites more in depth at the optimum T_d of 125°C.

3.1.2. Influence of flax content on α crystals as a function of various annealing periods at optimum crystal growth temperature

Figure 6 shows the melting curves of PLLA-F0 and PLLA-F10 (PLLA-F5 was also measured but not shown for clarity) for various annealing periods at the crystal growth temperature of 125°C. The minimum annealing time required to induce visible melting at this temperature is at least 5s in the case pure PLLA, whereas for PLLA-F10, crystals are present even after 1s, clearly showing that flax strongly enhances the crystallization rate at this optimal temperature. Increasing annealing times up to 2000s were tested to evaluate the influence of flax on the time to reach saturation of the degree of crystallinity, this time being of major importance for practical applications of the composites (see below, Section 3.6). Figure 6 shows this time is about 600s for neat PLLA but is reduced to 30s for PLLA-F10, a spectacular improvement.

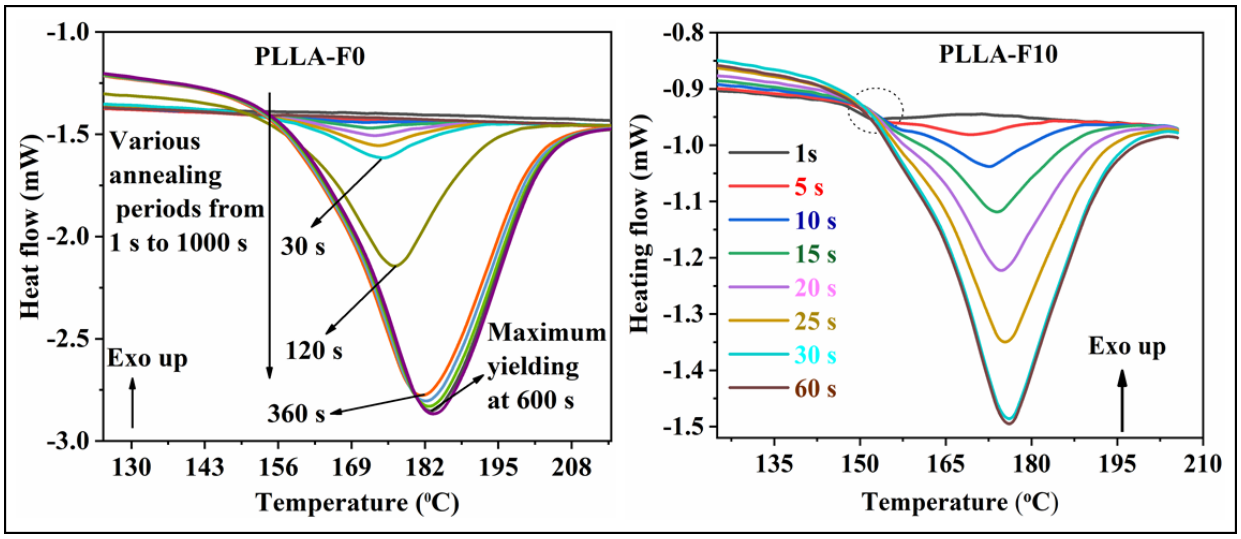

Figure 6

Melting peaks of PLLA-F0 and PLLA-F10 after isothermal crystal nucleation at 70°C for 360s followed by various annealing periods of crystal growth at 125°C.

Next, Figure 7 illustrates the influence of flax content on (a) the crystalline fraction taken as the melting enthalpy divided by the melting enthalpy of the pure α crystal and (b) the amorphous to semi crystalline converted fraction taken as the melting enthalpy divided by the melting enthalpy

at saturation, as a function of the annealing period at temperature 125°C after isothermal crystal nucleation at 70°C for 360s (protocol 2 on Figure 2b). The saturated degrees of crystallinity, crystallization rates and corresponding melting peaks show a strong influence of flax, consistent with Figure 6.

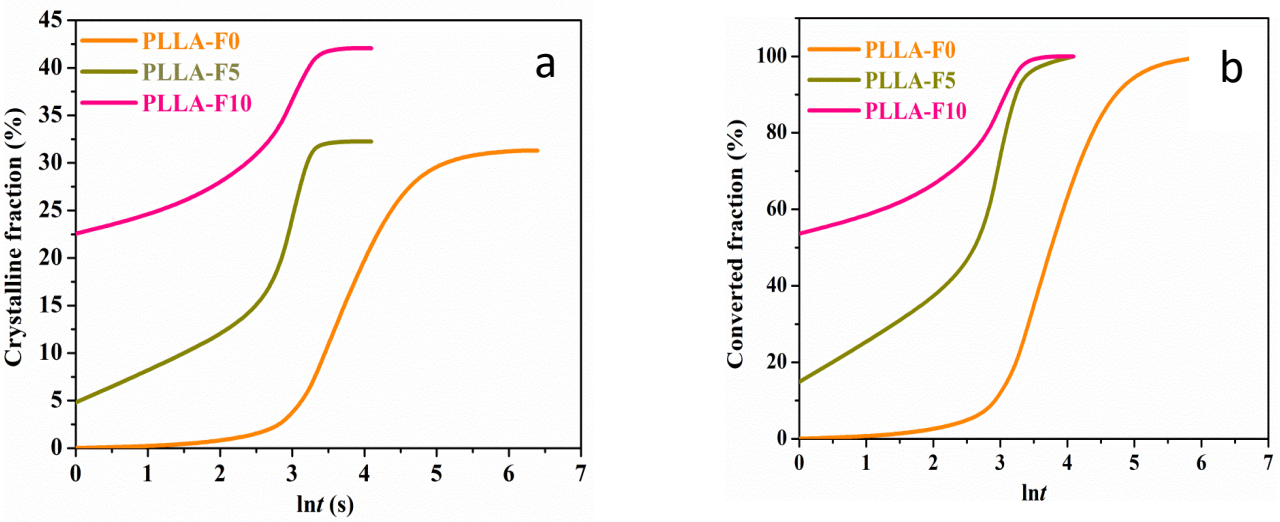

Figure 7

Influence of flax content on (a) the degree of crystallinity and (b) the amorphous to semi crystalline converted fraction deduced from the melting curves (see Figure. 6) after isothermal crystal nucleation at 70°C for 360s followed by crystal for up to 600s at 125°C.

3.2. Avrami analysis

The Avrami equation [40–42] is able to model isothermal phase transformations of solid materials through a nucleation and growth mechanism with progressive inpingement of the new phase domains. It expresses as :

$$\chi(t) = \chi_\infty[1 - exp(-kt^n)], \quad (1)$$

where $\chi(t)$ is the crystallinity at time t; χ_∞ is the crystallinity after the end of the (primary) crystallization process; k is the overall kinetic rate constant and n is the Avrami exponent, which depends on the nucleation and growth mechanisms of the crystal.

The Avrami analysis is extensively used to describe the isothermal crystallization of polymers from the melt. Additionally, if the volumic density of nuclei can be considered as fixed during crystallization (so-called instantaneous nucleation), which is the case during the crystal growth stage of a Tammann two-step annealing, it can been used to identify the growth dimensionality of the crystals, including the influence of a nucleating agent such as flax, provided that only one crystal form, and hence a single crystal growth rate, is present (α in our case).

The time evolution of the phase transformation is usually reported as the semi-crystalline fraction ($\gamma(t)$), which can be expressed as the ratio of the crystallization enthalpy at time t (ΔH_t) to the final crystallization enthalpy (ΔH_∞), both determined by DSC as

$$\gamma = \frac{\chi_t}{\chi_\infty} = \frac{\Delta H_t}{\Delta H_\infty} \quad (2)$$

Taking the double logarithm of Equation (1) and using equation (2) gives

$$\ln[-\ln(1 - \gamma_t)] = \ln(k) + n\ln(t) \quad (3)$$

Figure 8 shows the good fit of the experimental data with the Avrami equation in this linearized representation for T_d = 125°C. Indeed, the relationship is linear over a significant range of crystallinity and time for all samples. From the slope and intercept of the curves, the Avrami exponent n and rate constant k can be determined as also reported in Figure 8.

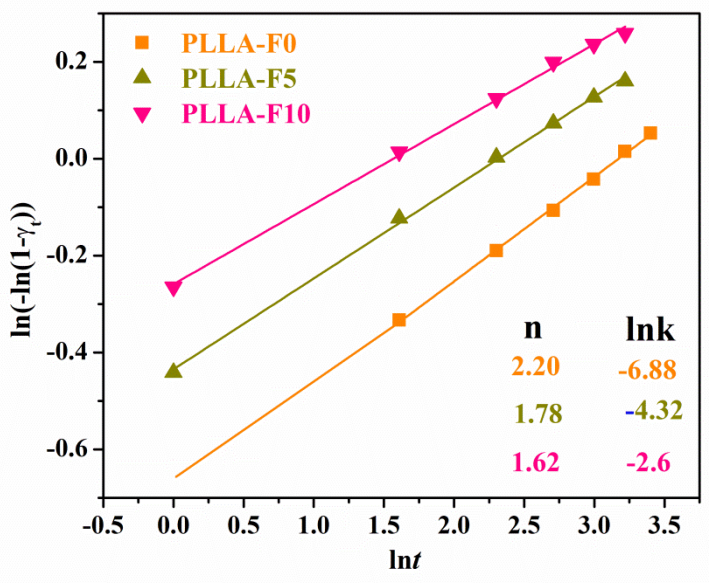

Figure 8

Linearized Avrami plots, including n and ln*k parameters of neat PLLA and PLLA-flax composites at isothermal crystal growth temperature of 125°C. The time range of the included data has been restricted to the linear dependence zone.*

The physical interpretation of the Avrami constants *k* and *n* is complex in the general case and open to discussion because the experimental data usually combine the stages of crystal nucleation and growth. If the nuclei are pre-formed, however, and thus present from the beginning, the transformation is only due to the *n*-dimensional growth of the crystals. Spherulitic growth unhindered in three dimensions from a pre-nucleated melt yields $n = 3$. In this study, the dimensionality of the crystals is clearly smaller even in the case of neat PLLA, which is a little above 2. This result is probably influenced by the minute thickness of the FDSC samples, preventing full 3D growth but is however also consistent with the morphological observations reported in Section 3.4 on fracture surfaces. An interesting condition occurs when the pre-formed nuclei densely populate preferred sites such as the surface of fibers and hinder the free growth of the spherulites in the lateral direction. This is the probable explanation for the significant reduction of *n* at high flax concentration and is further confirmed by optical microscopy observations in Section 3.4, although the limiting value of 1 is definitely not reached yet (n= 1.78 and 1.62 for PLLA-F5 and PLLA-F10 respectively). The faster crystallization at increasing flax content is clearly visible on the figure as well.

3.4. Crystal morphology

The influence of flax content on the PLLA crystal morphology of two-step crystallized samples (nucleation at 70°C for 360s followed by a crystal growth at 125°C for 600s) has been studied by polarized optical microscopy (POM). The micrographs are shown in Figure 9. The presence of flax fibers has a major influence on the crystalline morphology. The isotropic spherulitic structure can be observed for neat PLLA while trans-crystallization at the fibers surface is dominant for the composites.

The spherulite size of neat PLLA is quite large, up to 450μm in diameter as shown in Figure. 9a. Moreover, instantaneous nucleation can be inferred from the similar diameter of all spherulites as expected from the crystallization protocol. With increasing flax concentration, the final crystal size is gradually reduced down to 100 μm for PLLA-F10 because of the increased nucleation density. Most spherulites originate from the fiber surface in the composites, as shown in Figures. 9b–e. Nucleation sites are predominantly found at defects on the fibers, as shown in Figures. 9d and e, such as at the broken edges and knots along the fibers. Crystals also originate at fiber kinks. This is a classical result because defects increase the surface energy and hence stabilize nuclei. A similar mechanism was reported recently for various fiber-reinforced PLLA composites. [31-34]

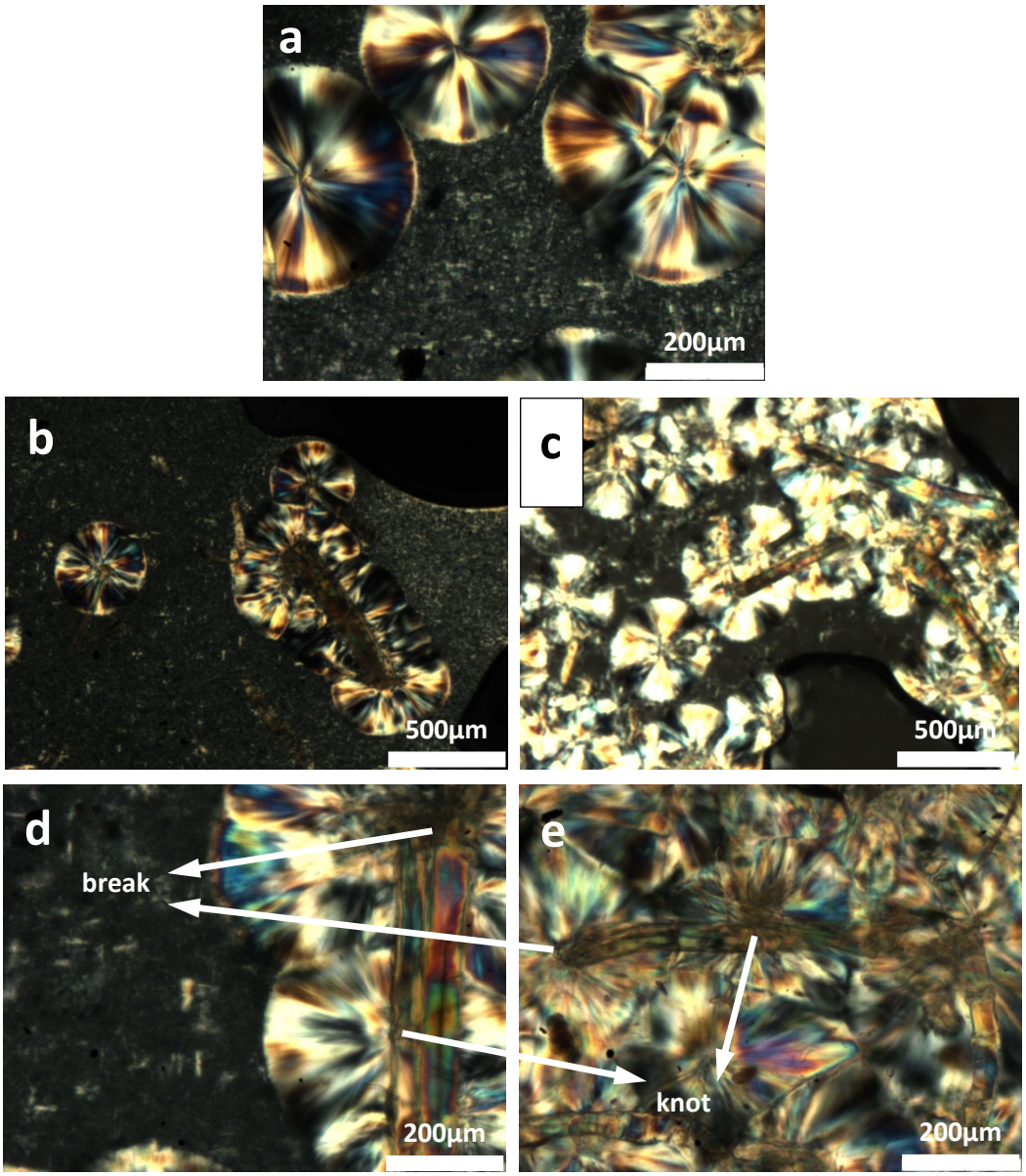

Figure 9

POM micrographs of neat and composite samples after isothermal nucleation at 70°C for 360s followed by crystal growth at 125°C for 600s.: a. PLLA-F0, b and d. PLLA-F1, c. PLLA-F5, e. PLLA-F10.

3. 5. Fracture surface morphologies of tensile test specimens

Figure 10 shows SEM micrographs of the fracture surfaces after tensile tests of as-molded and two-stage annealed samples of neat PLLA and PLLA-flax composites.

A clear imprint of bulk spherulites is found on the fracture surfaces of PLLA-F0 as illustrated in Figure 10a. The spherulites appear very flat, which suggests a growth dimensionality below 3 but above 2, consistent with the Avrami analysis reported above. Failure of fiber-reinforced composites is attributed in literature to a wide variety of mechanisms, including micro-voiding, cavitation, crazing, shear bending and yielding debonding, fiber pullout and breakage [43, 44]. In our case, fiber pullout and debonding are essentially absent. Minor voiding is observed in double-stage annealed samples (Figure 10e) but is related to the large contraction of the matrix upon crystallization. Excellent dispersion at the elementary fiber level (10-30 μm) is evidenced on all micrographs. As molded composites (Figure 10c and d) show even stronger interfaces than those reported recently by Aliotta et al. [45] on similar injection-molded PLLA-flax composites. This is probably because the fibers used in our work have been treated to improve compatibility with polyesters. When the crack tip is close to the fiber-matrix interface, it propagates cohesively in the matrix, not adhesively, which is consistent with the "Pukanszki model" analysis performed by Aliotta et al. [45] . In the two-stage crystallized composites, similar *close to interface* cohesive fracture patterns are observed as well, but in addition, there is a surprisingly large fraction of torn fibers with clear indication of fibrillation involving the separation of nanofibrils (Figure 10e and f). All these elements point towards a very strong fiber-matrix interface, which is fully consistent with the thermal and POM studies reported above. Although much less obvious than in the POM micrographs, trans-crystallization on the fibers surface can be detected as well upon careful observation.

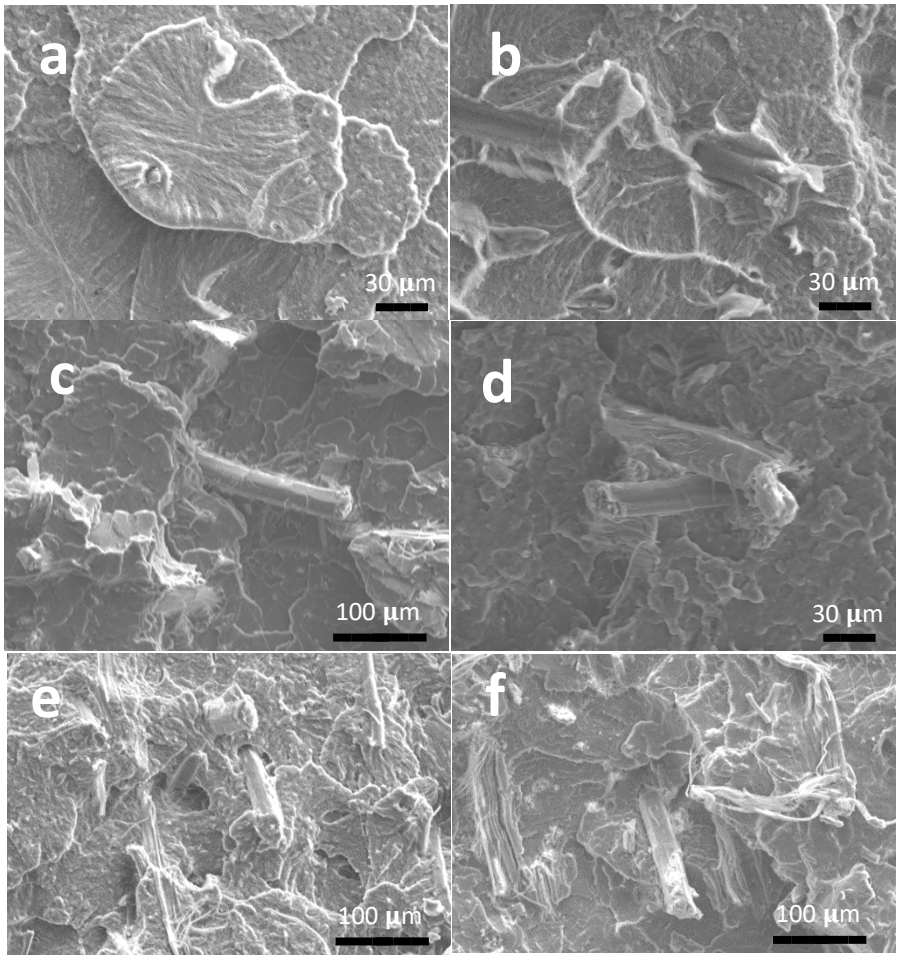

Figure 10

SEM micrographs of fracture surfaces of as-molded and two-step-annealed PLLA and composites.

(a) annealed PLLA-F0: spherulite imprint; (b) annealed PLLA-F1: spherulite nucleation site visible at the edge of fiber on the right; (c) as molded PLLA-F5; (d) as-molded PLLA-F10; (e) annealed PLLA-F5; (f) annealed PLLA-F10.

3.6. Dynamic Mechanical Thermal Analysis (DMTA), tensile and hardness tests

Based on the FDSC findings, a two-stage annealing treatment was applied to the DMTA and tensile test specimens obtained from injection molded parts, consisting of an isothermal nucleation step at 70°C for 360s followed by a crystal growth step at 125°C for 600s. From the FDSC results, the

annealing time at 125°C could be reduced for the composites, which would be advantageous from a technological standpoint, but the longer annealing time was preferred for consistency reasons, as it is required for neat PLLA. The effect of flax concentration on the modulus of PLLA-flax composites compared to neat PLLA is presented in Figure 11. DMTA results show both typical storage modulus (E) and damping behavior (tan δ) as a function of the temperature. The storage modulus of the neat PLLA is about 3.2GPa in the glassy region (room temperature). Consistent with literature, [19, 44, 45] this value significantly increases with increasing flax fiber content because of the higher polymer crystallinity (see Figure 5 and 8), the intrinsic contribution of the fibers stiffness and the strong flax-PLLA cohesion exhibited by the fracture surfaces (see Figure 10e and f). In particular, PLLA-F10 shows a remarkable 250% increase in storage modulus compared to the virgin PLLA, which is discussed below.

Tan δ curves are also shown in Figure 11b. The temperature at maximum tan δ is referred to as the dynamic T_g of the system. The dynamic T_g is shifted from 78°C to 82°C with increasing flax content, reflecting the lower mobility of the chains in the amorphous regions (shorter tie segments) and the damping peak height is significantly lowered due to the reduced mobile amorphous fraction at high crystallinity.

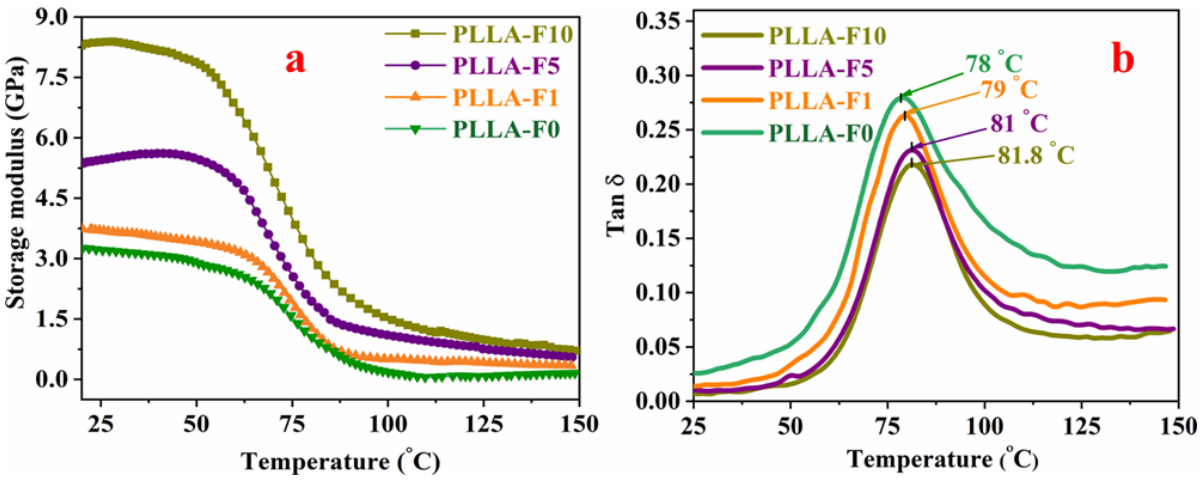

Figure 11

Effect of flax content on (a) storage modulus and (b) tan δ of two-stage-annealed samples at T_{nu} 70°C for 360s and T_d 125°C for 600s.

The tensile moduli, yield strength and elongation at break of as-molded and two-stage annealed test specimens are reported in Table 1. The corresponding strain-stress curves for two-stage annealed samples are shown in Figure 12-left. The numerical values as well as the overall shape of the curves for the as-molded samples are very consistent with literature. [4, 45] On the other hand, the tensile moduli of the two-stage annealed systems are exceptional and confirm the DMTA storage moduli values discussed above, more than twice as high for PLLA-F10.

The experimental values obtained by DMTA and tensile tests have been compared with the theoretical upper and lower bounds for the elastic modulus of composites, namely the Voigt and Reuss models expressed as:

Voigt model

$$E_c = E_f \phi_f + E_m \phi_m \tag{4}$$

Reuss model

$$\frac{1}{E_c} = \frac{\phi_m}{E_m} + \frac{\phi_f}{E_f} \tag{5}$$

where E_c is the composite modulus, E_m is the (PLLA) matrix modulus, E_f is the flax fiber (filler), modulus, ϕ_m and ϕ_f are the volume fractions of matrix and filler, respectively.

The Voigt model (Eq. 4) represents the ideal situation where the stiff component (here flax fibers) carries the maximum load possible as a result of a full transfer of the applied deformation, meaning their aspect ratio is high and they are oriented parallel to the main loading direction. The Reuss model (Eq. 5), by contrast, describes the most compliant composite arrangement possible, as if the stiff component were arranged as platelets perpendicular to the main loading direction. The modulus of any fiber-polymer composite should be comprised between these two boundaries in the absence of porosity and other significant internal flaws. [46,47]

The weight fractions (wt%) have been converted to volumetric fractions (ϕ) based on literature data: 10% w/w flax in PLLA corresponds to 8.9% v/v. The average fiber modulus E_f is taken as 60GPa, a consensus value obtained by different laboratories using the impregnated fiber

bundle test (IFBT) for the same batch of fibers. [48] The modulus of PLLA is taken as E_m=3.2GPa obtained by DMTA of two-step annealed samples. Figure 12-right shows experimental data points with error bars and the mechanical model lines of E_c as a function of the fiber ϕ. Table 1 shows the corresponding numerical values.

Table 1

Tensile data of as-molded and annealed samples and Vickers Hardness of annealed samples

(standard deviations between brackets below the averages)

	Tensile modulus [GPa]		**Tensile yield strength [MPa]**		**Elongation at break [%]**		**Hardness [MPa]**	
	As molded	*Annealed*	*As molded*	*Annealed*	*As molded*	*Annealed*	*1 kg load*	*10 kg load*
PLLA-F0	3.00 [0.21]	3.30 [0.19]	75,9 [0.29]	67,1 [0.45]	4,33 [0.06]	2,73 [0.10]	24,6 (*) [0.49]	24,0 [0.63]
PLLA-F1	3.12 [0.20]	3.75 [0.19]	73,4 [0.34]	62,7 [0.29]	3,32 [0.10]	2,57 [0.09]	24,6 [0.55]	23,2 [0.21]
PLLA-F5	3.58 [0.19]	5.26 [0.20]	71,8 [0.45]	62,5 [0.50]	3,21 [0.09]	1,99 [0.06]	24,7 [0.31]	23,1 [0.60]
PLLA-F10	4.18 [0.22]	8.01 [0.18]	71,7 [0.32]	60,5 [0.34]	2,39 [0.07]	1,20 [0.08]	22,0 (*) [0.55]	20,5 [0.30]

(*) average of perpendicular and parallel measurements, one std dev. intervals overlapping

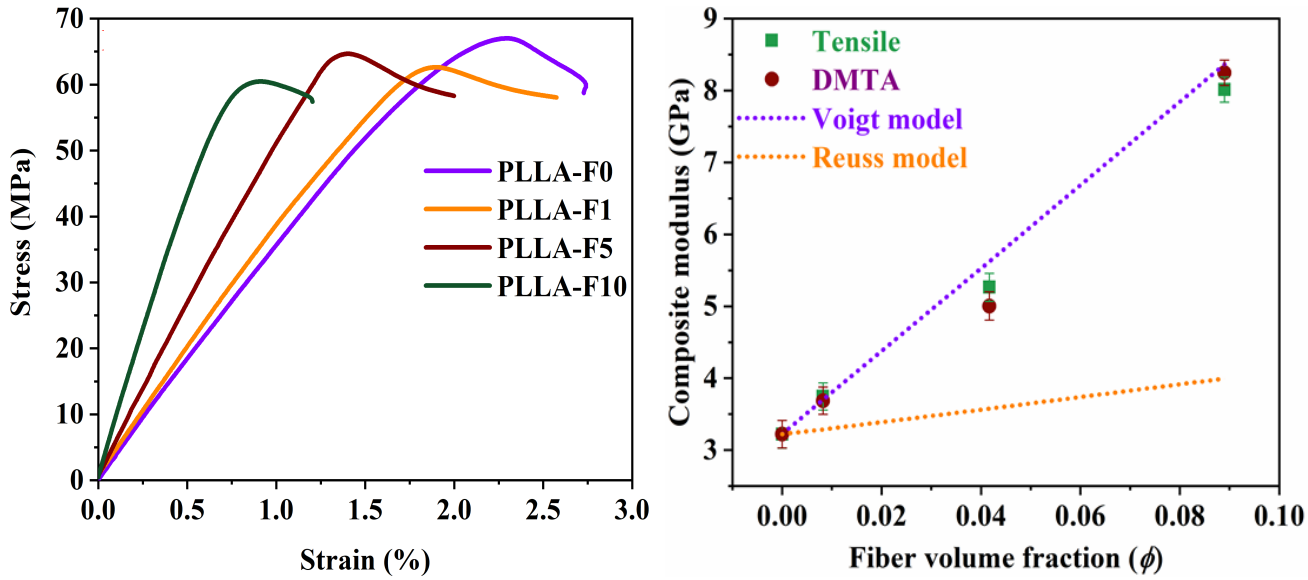

Figure 12

Experimental and model tensile values of PLLA and flax composites at 25°C as a function of the fiber fraction. Samples have been two-stage annealed at T_{nu} 70°C for 360s and at T_d 125°C for 600s before measurements.

Left: stress-strain curves; right: Storage and tensile moduli.

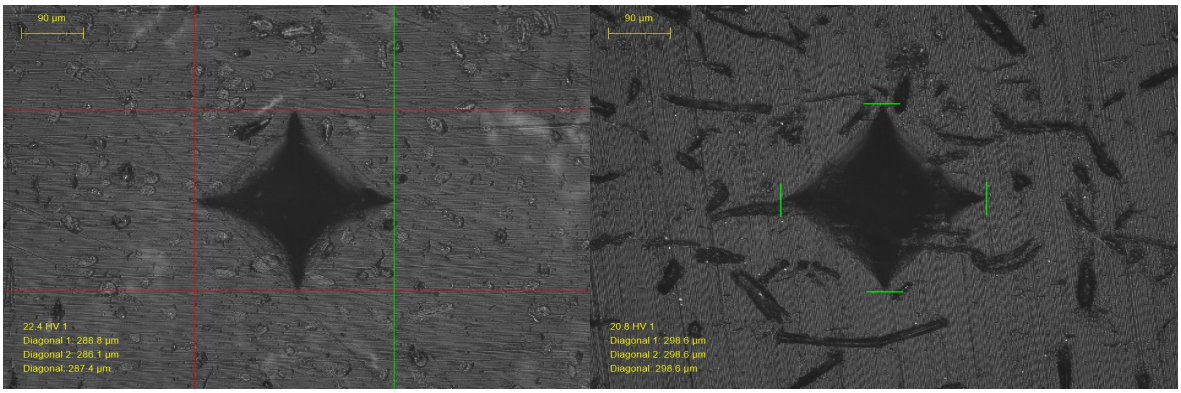

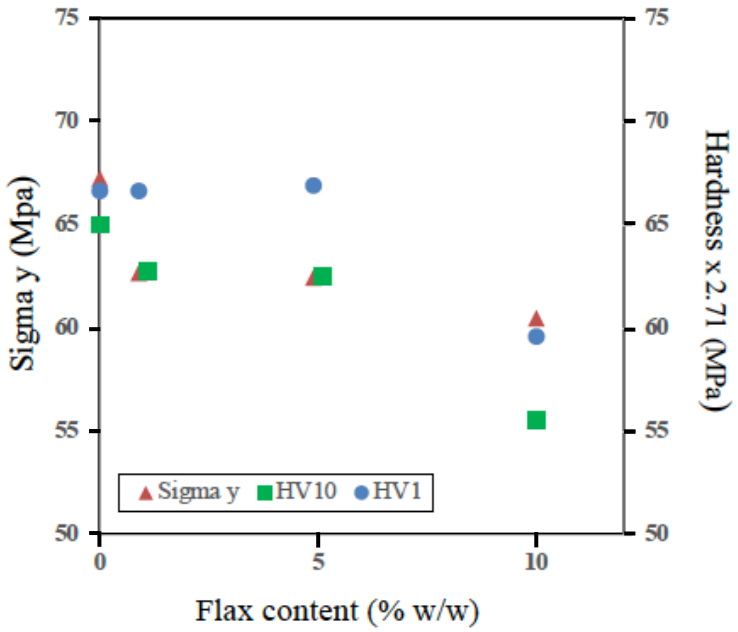

Figure 13

Hardness results and comparison with tensile strength:

Top: Micrographs of polished sections of annealed PLLA F10 tensile bars cut in the middle, after indentation at 1kg. Scale bars = 90 micrometers.

Top left: section perpendicular to the long dimension of test specimen. Top right: section parallel to the long dimension of test specimen and perpendicular to sample thickness.

Bottom: Comparison of tensile yield strength and rescaled hardness as a function of flax weight content. Hardness data multiplied by factor 2.71, see text for details.

The experimental E_c values are very close to the Voigt model. This is quite unusual for such a class of composites as it suggests that the fibers indeed carry the maximum load possible. The experimental result itself is in little doubt since:

(i) the modulus values come from two independent techniques, one quasi static, the other dynamic and the data analysis methods of the two are uncorrelated,
(ii) the results show a fully consistent trend for all compositions,
(iii) for each composition, there is a statistical validation on several test pieces and the standard deviations reported in Tables 1 are low (Table 1 and Figure 12-right).

Because the result is quite exceptional, it calls for a credible explanation at the microscopic level, which is done below, based on inspection of Figures 10 and 13-top:

(i) the fibers are extremely well dispersed in the matrix, at the elementary fibers level, as confirmed by SEM on fracture surfaces and optical microscopy on polished sections cut in the middle either perpendicularly or parallel to the long dimension (Figures 10 and 13top),
(ii) the fibers are strongly adhering to the matrix after the double annealing procedure, much more so than after a more usual crystallization procedure, to the point they fracture rather than detach from the matrix (Figure 10); this leads to excellent load transfer due to a perfect cohesion with the matrix,
(iii) the pneumatic injection process molding generates very high shear in the narrow central part of the test specimens and favors alignment of the fibers along the flow, i.e. in the test specimens length direction (Figure 13 top left and right),
(iv) the flax fibers are tough and flexible; they retain a very high aspect ratio during processing, in excess of 10 (Figure 13 top right), as opposed e.g. to brittle glass fibers,
(v) the overall effect is to yield a modulus close to a UD continuous fibers composite in the fiber alignment direction.

The tensile strength of the as-molded samples (Table 1) is comprised between about 77 and 72MPa, with a moderately decreasing trend at increasing flax concentration. These results are coherent with (the higher end of) literature data on short fibers PLLA-flax composites. [4, 45] Rather

surprisingly (and disappointingly), the tensile strength of the double annealed samples is lower than that of the as-molded samples by 8.7 to 11.2 MPa, with no systematic trend as a function of flax content. Additional fiber or matrix thermal degradation specifically caused by the double annealing can be excluded since the extra thermal treatment is well within the thermal stability limits of the fibers and the matrix, especially taking into account that the fibers used in this work have a low hemicellulose content (around 5%, see Supplementary Information), compared to the usual green or retted fibers, [49] hemicellulose being the fibers component with the lowest thermal stability. As detailed in the Supplementary Information (Section S2), significant matrix hydrolysis during extrusion, molding and annealing is also unlikely. The most probable explanation is that the two-stage annealing treatment leading to high crystallinity of the matrix also generates a lot of tensile stresses around the fibers due to the large shrinkage mismatch between the matrix and the fibers. These stresses facilitate the propagation of cracks initiated in the matrix even through the fibers by a fiber splitting mechanism, compatible with the SEM observations (Figure 10e and f).

Since the tensile test specimens tend to break in the shoulder area and thus the measured strength might be limited by the imperfect alignment of the fibers in this zone (see Figure 10), the tensile tests were complemented by Vickers microhardness measurements at 1 and 10kg load (HV1 and HV10 resp.) on polished sections close to the center of the test pieces, either perpendicular or parallel to the long dimension. The results are summarized in Table 1. The microhardness values are fully consistent with the tensile strength. The best strength to hardness ratio to superimpose the datasets is 2.71+/-0.13 (all results are included). This ratio is close to the central value for polymer-based materials.[50] Moreover, the microhardness values are independent of the indented surface orientation within experimental errors, meaning that the strength of the composites is controlled by the matrix, even in the case of the highly crystalline two-stage annealed samples despite their very strong interface and high anisotropy. The strength and rescaled hardness results are summarized in Figure 13-bottom. The figure confirms the negative influence of flax on strength or hardness and highlights a statistically significant difference between the HV1 and HV10 values. The lower load hardness being higher suggests an indentation depth effect, with the surface harder than the bulk by about 5%.[51] Interpretation of this result is beyond the scope of this article.

Finally, as expected, the elongation at break is negatively influenced by both two-step annealing and increasing flax concentration (Figure 12-left and Table 1). However, even PLLA-F10 after two-step annealing shows a true yield and a short softening plastic deformation zone,

despite its very high modulus. Such compositions might find use in moderately demanding applications such as snap-fits. It is further interesting to notice that few materials are available in the range of specific stiffness provided by PLLA F10.

4. **Conclusions**

In summary, the Tammann protocol that cleanly separates the nucleation and crystal growth stages of polymer crystallization combined with the use of ultra-fast DSC, has enabled unraveling the influence of flax fibers on the thermal and mechanical properties of injection-molded PLLA-flax composites. The main findings of this study are:

- Flax fibers are very efficient and selective nucleating agents of PLLA favoring the ordered α phase and speeding up crystallization by a factor 20 at 10 wt/wt flax content. Their influence is unambiguously demonstrated by microscopy and thermal analysis: effective trans-crystallization is observed at the fibers surface, leading to a reduction of the crystal growth dimensionality as shown by Avrami analysis.
- Matrix degradation by hydrolysis during extrusion owing to the hygroscopic nature of the fibers is unlikely to play a significant role in the studied composites thermal behavior.
- The extensive trans-crystallization on the fibers surface, the very strong fiber-matrix interface, the preservation of a high fiber aspect ratio after extrusion and molding and the almost perfect fibers alignment result together in remarkable stiffness of Tamman- annealed composites since the obtained modulus is close to the Voigt model theoretical maximum.
- The excellent fiber dispersion at the elementary fibers level offers perspectives to obtain extremely stiff composites at higher fiber load, in a range of specific modulus difficult to achieve otherwise.

Acknowledgments

WB, VD and RN acknowledge financial support by FEDER (Low Carbon Footprint Materials portfolio, MACOBIO project)

References

[1] M. J, John, Thomas, S., *Carbohydrate polymers.* **2008,** *71,* 343-364.

[2] O. Faruk, A. K. Bledzki, H. P. Fink, M. Sain, *Prog. Polym. Sci*. **2012**, *37,* 1552-1596.

[3] A. K. Mohanty, M. Misra, L. T. Drzal, *Natural Fibers, Biopolymers and Biocomposites*, CRC press, Boca Raton, FL, **2005**

[4] L. Yan, N. Chouw, K. Jayaraman, *Comp. Part B: Eng.* **2014**, *56,* 296-317.

[5] C. Baley, *Compos. A. Appl. Sci. Manuf.* **2002**,*33,* 939–948.

[6] R. A. Auras, L. T. Lim, S. E. Selke, H. Tsuji, *Poly(lactic acid): Synthesis, Structures, Properties, Processing, and Applications*, John Wiley & Sons: Hoboken, NJ. **2010**

[7] M. L. Di Lorenzo, R. Androsch, *Polym Intern*. **2019**, *68*, 320-334.

[8] R. Vasanthakumari, A. J. Pennings, *Polymer*. **1983,** *24,* 175-178.

[9] P. De Santis, A. J. Kovacs, *Biopolymers*. **1968**, *6,* 299–306.

[10] M. Cocca, M. L. Di Lorenzo, M. Malinconico, *Europ. Polym. J.* **2011**, *47*, 1073-1080.

[11] H. Tsuji, Y. Ikada, *Polymer*. **1995**, *36,* 2709-2716.

[12] Z. Chengbo, H. Guo, J. Li, S. Huang, H. Li, Y. Meng, D. Yu, C. Jesper de Claville, S. Jiang, Rsc. *Adv.* **2016,** *6*, 113762-113772.

[13] B. Wang, W, Tao, X. Zhang, A. Tercjak, X. Dong, A. J. Müller, D. Wang, D. Cavallo, *Macromolecules*. **2019**, *52*, 6274-6284.

[14] R. Zhao, X. Zhou, G. Dai, *Polym. Composites*. **2002**, *23,* 1026−1035.

[15] J.C. Halpin, J. L. Kardos, *J. App. Phy.***1972**, *43* 2235-2241.

[16] A. Arias, M. C. Heuzey, M. A. Huneault, *Cellulose.* **2013**, *20,* 439-452.

[17] E. Nassiopoulos, J. Njuguna, *Materials & Design.* **2015**, *66*, 473-485.

[18] X. Xuezhu, F. Liu, L. Jiang, J. Y. Zhu, D. Haagenson, P. D. Wiesenborn, *appl. Mater. Int.* **2013**, *5,* 2999-3009.

[19] T. Gao, Z.M. Zhang, L. Li, R.Y. Bao, Z.Y. Liu, B.H. Xie, M.B. Yang, W. Yang, *Appl. Mater. Int.* **2018,** *10,* 20044-20054.

[20] H. Shaoyong, H. Li, S. Jiang, X. Chen, A. Lijia, *Polymer*. **2011**, *52*, 3478-3487.

[21] L. Cartiera, T. Okiharaa, Y. Ikadab, H. Tsujic, J. Puiggalia, B. Lotza, *Polymer*. **2000**, *41*, 8909–8919.

[22] G. Stoclet, R. Seguela, J. M. Lefebvre, S. Elkoun, C. Vanmansart, *Macromolecules.* **2010**, *43*, 1488–1498.

[23] Z. Jianming, Y. Duan, H. Sato, H. Tsuji, I. Noda, S. Yan, Y. Ozaki, *Macromolecules.* **2005**, *19*, 8012-8021.

[24] Z. Jianming, K. Tashiro, H. Tsuji, J.D. Abraham, *Macromolecules.* **2008**, *41,* 352-1357.

[25] M.C. Righetti, M. Gazzano, M.L. Di Lorenzo, R. Androsch, *Eur. Polym. J*., **2015**,*70*, 215-220.

[26] A. Toda, R. Androsch, C. Schick, *Polymer.* **2016**, *91*, 239–263.

[27] Z.L. Li, D.S. Zhou, W.B. Hu, *Acta Polym. Sin.* **2016**, 9, 1179–1197.

[28] V. Mathot, C. Schick, *Fast Scanning Calorimetry*, Springer International Publishing, Switzerland, **2016**

[29]. R. Androsch, C. Schick, M.L. Di Lorenzo *Macromol. Chem. Phys.* **2014**, *215*, 134–1139.

[30] R. Androsch, E. Zhuravlev, S. Christoph, *Polymer.* **2014**, 55, 4932–4941

[31] M. G. Huson, W. J. McGill, *J. Polym. Sci. Polym. Chem. Edi.* **1984**, *22*, 3571-3580.

[32] T. Liu, Y. Xuejiang, Y. Fengmei, X. Zhao, A. Lu, J. Wang, W. Xianzhong, L. Tianli, *Polym. Plast. Tech . Eng*, 51: 597–604, 2012

[33] B. Wang,† T. Wen,‡ X. Zhang,§ A. Tercjak,‖ X. Dong,‡ A. J. Müller,⊥,# D. Wang, and D. Cavallo, *Macromolecules*. **2019**, *52*, 6274−6284

[34] D.R. He, Y.M, Wang, C.G, Shao, G.Q. Zhang, Q. Li, C.Y. Shen, *Polym Test.* **2013**, *32*, 1088–1093

[35] T. Hata, K. Ohsaka, T. Yamada, K. Nakamae, N. Shibata, T. Matsumoto, *J. Adhes*. **1994**, *45*, 125−135.

[36] G. Tammann, *j. Phys. Chem.* **1898**, *25,* 441–479.

[37] E. Zhuravlev, J.W. Schmelzer, A.S. Abyzov, V.M. Fokin, R. Androsch, C. Schick, *Crystal Growth & Design,* **2015,** *15*, 786-798.

[38] E. Zhuravlev, J.W. Schmelzer, R. Androsch, C. Schick, *Int. Polym. Proc.* **2016**, *31*, 628-637.

[39] R.A. Andrianov, R. Androsch, R. Zhang, T.A. Mukhametzyanov, A.S. Abyzov, J.W. Schmelzer, C. Schick, *Polymer.* **2020**, 122453.

[40] M. Avrami, *J. Chem. Phy.* **1939**, *7*, 1103–1112.

[41] M. Avrami, *J. Chem. Phy.* **1940**, *8*, 212–224.

[42] M. Avrami: *J. Chem. Phy.* **1941**, *9,* 177–184.

[43] S.D. Park, M. Todo, K. Arakawa, *Trans Tech Publications Ltd.* **2004**, *261,* 105-110.

[44] S.D. Park, M. Todo, K. Arakawa, *J. mater. Sci.* **2004**, *39*, 113-1116.

[45] L.Aliotta, V.Gigante, M.B.Coltelli, P.Cinelli, A. Lazzeri, M. Seggiani, *Appl. Sci.,* **2019**, *9*, 3797.

[46] D. Battegazzore, J. Alongi, A. Frache, *J. Polym. Envi.* **2014**, *22*, 88-98.

[47] E. Hablot, R. Matadi, S. Ahzi, L. Avérous, *Comp. Sci. Techn.* **2010**, *70,* 504-9.

[48] F. Bensadoun. *Master Thesis*, Katholieke Universiteit Leuven **2016**.

[49] J. George, E.T.J. Klompen, T. Peijs, *Adv. Comp. Let.*, **2001**, *10*, 81-88.

[50] A. Clausner, F. Richter*, Eur. J. Mech. Solid*. **2015**, *51,*11–20.

[51] T. Koch, S. Seidler, *Polym. Strain,* **2008,** *45*, 26–33.

Appendix: Supporting Information

S1. Detailed Experimental Section

S1.1. Materials

Non-crimp Unidirectional (UD) flax fibers (AmpliTex ® UD type 5057) were provided by Bcomp® (Fribourg, Switzerland). According to the manufacturer, these UD fabrics have excellent compatibility with polyesters and are suitable for extrusion-based processes and molding. As-received fabrics were finely chopped into discrete fibers with0.4-0.5 mm length as shown in Figure S1. The chemical composition of flax fibers used in the current experimental investigation is given in Table S1.

Ingeo™ poly-lactic acid (PLLA) crystalline (grade 2500HP) was supplied in pellets form by *Nature Works LLC*. Table 2 summarizes the properties of this material.

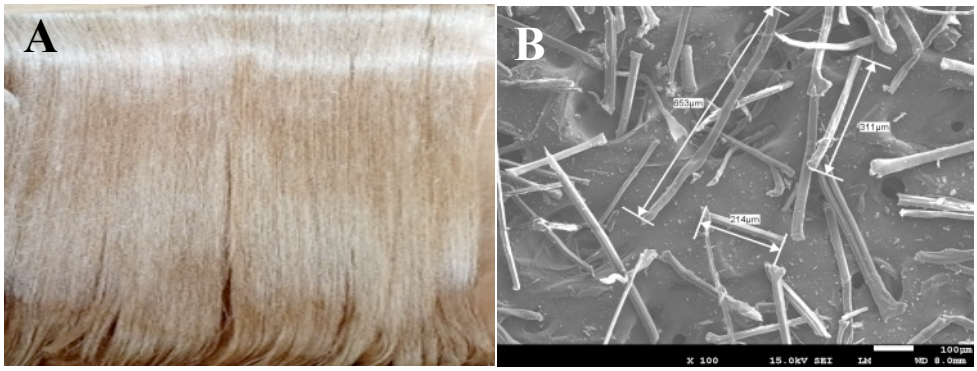

Figure S1

(A) Non-crimp unidirectional flax fibers mat and (B) Chopped fibers with average length 0.4-0.5 mm.

Table.S1

Chemical composition of flax fibers used in this work

Chemical composition	Weight (%)
Total solid content	87.5
Cellulose	70
Hemicellulose	5
Lignin	4
Pectin	2
Moisture content	12.5
Ash content	0.5
Others	3

Table S2

Properties of PLLA used in this work

Material	Properties with Units	Value	Standard/Method
PLLA	Density (g/cm^3)	1.24	ASTM D1505
	Melt flow rate (g/10 min) (210°C, 2.16kg)	8	ASTM 1238
	Tensile Strength (MPa)	65.5	ASTM D638
	Tensile Elongation (%)	4.3	ASTM D638
	Izod Impact (J/m)	40	ASTM D256
	Flexural Strength, (MPa)	126	ASTM D790
	Flexural Modulus (MPa)	4350	ASTM D790

S1.2. Processing of the bio-composites

The chopped fibers were dried at 105°C under vacuum for 12 hours to remove moisture. In order to prevent polymer degradation by hydrolysis during extrusion, the as received PLLA was dried at 60°C under vacuum overnight. The processing conditions recommended in the *Nature Works* technical data sheet were followed.

Table S3 shows the composition of the samples used in this study. PLLA/flax blends were compounded in a Thermo Scientific Process 11 co-rotating twin screw extruder. Dried PLLA pellets and chopped fibers were first pre-mixed by hand and next fed into the hopper of the machine. The set temperature profile of the heating zones (T_2 to T_8) ranged from 190 to 210°C from hopper to die and the screw speed was 150 rpm. The residence time in the extruder was around 1 min. The extruded composite strands were immediately quenched in cold water and pelletized. The pellets were dried for 6 hrs at 60 °C before injection molding.

Dried compounded pellets were injection-molded (IM) to produce dog-bone test pieces in a Thermo Scientific™ HAAKE™ MiniJet Pro. IM processing parameters were as follows: cylinder temperature 220°C, mould temperature 70°C, pressure 600 bar, post pressure 500 bar. The pressure and the post pressure were maintained for 30 seconds. Because the machine configuration only allows sequential injection and cooling of individual moldings from the melt stored in the reservoir, the residence time in the melt ranged from about 1 to 8 min to produce 4 test specimens. No significant difference between the samples mechanical properties was observed as a function of this residence time. Indeed, we found no drift of the properties reported in Table 1 as demonstrated by the low standard deviation values shown between square brackets below the averages.

Based on the FDSC findings (Section 3.1), a two-stage annealing treatment was applied to the injection-molded tensile bars, consisting of an isothermal nucleation step at 70°C for 360s followed by a crystal growth step at 125°C for 600s. The two annealing steps were carried out in vacuo right after molding the entire batch of test pieces, in two neighboring ovens thermostated at the right temperatures. All test specimens were always dried (overnight at 60C) before mechanical testing.

Table S3

Nomenclature and composition of PLLA/Flax composites

Sample code	PLLA (wt%)	Flax (wt%)	PLLA/Fiber (vol./vol.%/%)
PLLA-F0	100	0	100/0
PLLA-F1	99	1	99.18/0.82
PLLA-F5	95	5	95.83/4.17
PLLA-F10	90	10	91.1/8.9

S1. 3. Characterization Techniques

S1.3.1. Fast-scanning chip-calorimeter (FDSC)

FDSC crystallization experiments, using Tammann's two stage nucleation and growth method, were performed on a Flash DSC 1 instrument from Mettler-Toledo connected to an intercooler and nitrogen purge gas. The calorimetric chip-sensor was conditioned three times and corrected one time according to the standard procedure prior to use. The samples were cut from extruded pellets into slivers with approximate thickness of 10 μm, lateral extension of about 150 μm and weight of about 100-250 ng with the help of a sharp razor. They were positioned at the center of the microchip sensor with the help of a hair. The mass (m) of such tiny samples is impossible to weigh on a conventional balance and is rather inferred for quantification of crystallinity by back calculation from comparison with a reference enthalpy value obtained on a conventional DSC for a sample of known weight:

$$m = \frac{\Delta H_t}{\Delta h_t} \quad (1)$$

with ΔH_t the melting enthalpy of the FDSC sample and Δh_t the specific melting enthalpy of the same composition obtained on a conventional DSC (in our case Mettler Toledo, model DSC1). The calculation is best based on "as comparable as possible" scan rates on the two instruments. The selected cooling rates were -0.16°C/s and -10°C/min for the FDSC and conventional DSC

respectively. Heating rates are less critical for fully crystallized samples and were 100°C/s and 10°C/min respectively.

The conversion from specific melting enthalpy to crystallinity is based on a ΔH_m^0 value of 107 J/g for the α′ and 143 J/g for the α forms respectively taken from [M.C. Righetti, M. Gazzano, M.L. Di Lorenzo, R. Androsch, Eur. Polym. J., **70**, 215, 2015].

The crystallinity values of composites samples has been corrected for fiber weight content by dividing the specific heat (with respect to *composite* sample weight) by the polymer weight fraction of that sample.

The question of the representativity of such small samples for the crystallization behavior of the bulk composites must further be addressed as well. Morphology results (Figures 10 and 13) validate the excellent dispersion of the reinforcement at the individual microfibers level. The fibers are moreover much longer than the Flash DSC sample thickness even after extrusion and molding (see Figure 13 top-right). The samples are taken from extruded pellets. Hence the fiber orientation is more or less random (low shear rate processing). In first approximation, the fiber volume fraction is close to the surface fraction. Elementary fibers have an average diameter of 15 microns. Their average inter-distance across the sample surface will be close to the square root of their surface or volume fraction. At 0,9 %, v/v, corresponding to 1% w/w (sample PLLA-F1), this distance is close to the lateral extension of the sample (150 microns). Hence, the representativity of PLLA-F1 is not guaranteed: only about 50% probability that one fiber is present in the slice. Hence, we have not included this sample in the Flash DSC results (with no impact on the overall conclusions). Fortunately, at 5 and 10% w/w the situation is quite different. The probability, that no fiber is present goes down to 3% and 0.1% respectively (i.e. "no fiber probability" approximately equal to $(½)^5$ and $(½)^{10}$ respectively). One fiber in a Flash DSC sample is enough to strongly influence nucleation since the average spherulite size of the selected neat PLLA (400 microns, see Figure 9a) is much larger than the Flash DSC sample size. This reassuring estimate combined with the smooth evolution of the crystallization rates with flax content (Figure 7 and 8) gives the needed confidence in the representativity of the samples containing 5 and 10% w/w flax.

S1.3.2. Dynamic mechanical thermal analysis (DMTA)

The viscoelastic properties of two-stage annealed composites were analyzed in tensile mode, using a DMA/SDTA861e DMTA by Mettler Toledo, equipped with a 40N load cell. At least two test specimens were obtained by cutting moldings to the desired average size (L*W*H = 9*4*2.5 mm) and were used after drying overnight at 60° in an oven *in vacuo*. The temperature range of the experiments was from 20 to 150 °C, with a heating rate of 3 °C/min, at a constant frequency of 1 Hz, maximum force of 2N and maximum displacement of 1μm, all well within the linear response.

S1.3.3. Tensile Tests

Tensile tests were carried out on as-molded and two-stage annealed composites. The samples previously dried overnight at 60° in an oven *in vacuo* were tested at room temperature with relative humidity of 50% on a Zwick Roell test machine at a crosshead speed of 5mm/min. At least five specimens for each composite were tested and the average values were reported.

S1.3.4. Microhardness Tests

Vickers microhardness tests were performed on an EMCO-test DuraScan G5 indentor machine equipped with a Vickers diamond tip on double-annealed test specimens at 1 and 10kg indentation force after 10s dwell time. The tensile samples were mounted and polished on SiC paper down to ultrafine P4000. The investigated surfaces were located at the very center of the sample. Both perpendicular and parallel to loading line sections were prepared in order to check the influence of fiber orientation and/or anisotropy. 16 indentation measurements (4 by 4 matrix) were performed on the studied sections with a load of 1 kg for the full series and 10 kg for selected samples.

S1.3.5. Polarized optical microscopy (POM)

Crystal morphologies were observed by POM on a AX70 microscope from Olympus coupled with a Mettler Toledo FP90 hot-stage. The neat PLLA and PLLA/flax composites were placed between two glass slides. Samples were first heated from 20 to 220 °C at 20°C/min and held at that temperature for 1min to allow complete melting, then cooled as fast as possible to 70°C for 6min in order to avoid any crystallization. Finally, the samples were heated to 125 °C during 10min.

S1.3.6. Scanning electron microscopy (SEM)

The fracture surfaces of the tensile specimens were analyzed by SEM on a JEOL 7600F instrument. A thin layer of gold (around 10 nm) was coated by sputtering on the surface of the composite specimens prior to observations.

S2. Potential issue of matrix degradation during processing, annealing and FDSC measurements of the composites

The FDSC samples were taken from extruded pellets as explained in Section S1.3.1. Hence only degradation during extrusion and analysis has to be taken into account. The matrix degradation of the composite samples could in principle come from thermo-oxidative instability, shear-induced degradation and hydrolysis. The first two routes are easily dismissed since (i) the chosen PLLA is a commercial grade and hence contains a thermal stabilizer package, (ii) only moderate processing temperatures compatible with the supplier recommendations are used and (iii) no evidence of shear overhearing has been observed during extrusion. The real question is hydrolysis since natural fibers are hygroscopic and polyesters are sensitive to high temperature hydrolysis if not "bone-dry." Hydrolysis during measurement in the Flash DSC can also be dismissed because of the very low thickness of the samples (around 10 microns), meaning water diffusion out of the samples only takes seconds at the crystallization temperatures (from 70 to 140°C). Hydrolysis of the composite test specimens during annealing is similarly unlikely because of the low temperatures and times involved (125°C for 10 min). The only remaining question is matrix hydrolysis during extrusion.

The manufacturer-recommended procedure was used to dry the polymer before extrusion (overnight at 60°C in vacuo) and a validated drying procedure was applied for the fibers as well (12h at 105°C in vacuo). The dry-mixed components were transferred as fast as possible from the drying ovens to the extruder. This is the best procedure available in our laboratory. To assess if this procedure guarantees the absence of degradation during extrusion of the matrix-fibers dry-blend, TGA experiments were performed on a small batch of chopped fibers, dried and undried. Figure S2 shows that the dried fibers pick up around 4.5% moisture in the short time (estimated at around 5 minutes) for the oven-to-extruder transfer, only slightly less than undried ones (6%). However, the experiments also show that the weakly physisorbed water picked up during fibers transfer or storage entirely evaporates between 60°C and 120°C. No additional weight loss is observed until

well above the extrusion temperature and time range (190°C-210°C for < 1 min), when cellulose dehydration reactions start taking place as well as degradation of other fiber components. Translating this result to the actual processing leads to the conclusion that the moisture adsorbed on the surface of the fibers quickly evaporates in the feeding section of the extruder, well before the melting and compacting stage and hence exits the extruder as vapor at the hopper without major degradation effect on the polymer. Industrial best practice would recommend placing a vent port in a partially filled section of the extruder between two melt plugs just after melting is complete in order to maximize water removal, but this setup is not available in our laboratory.

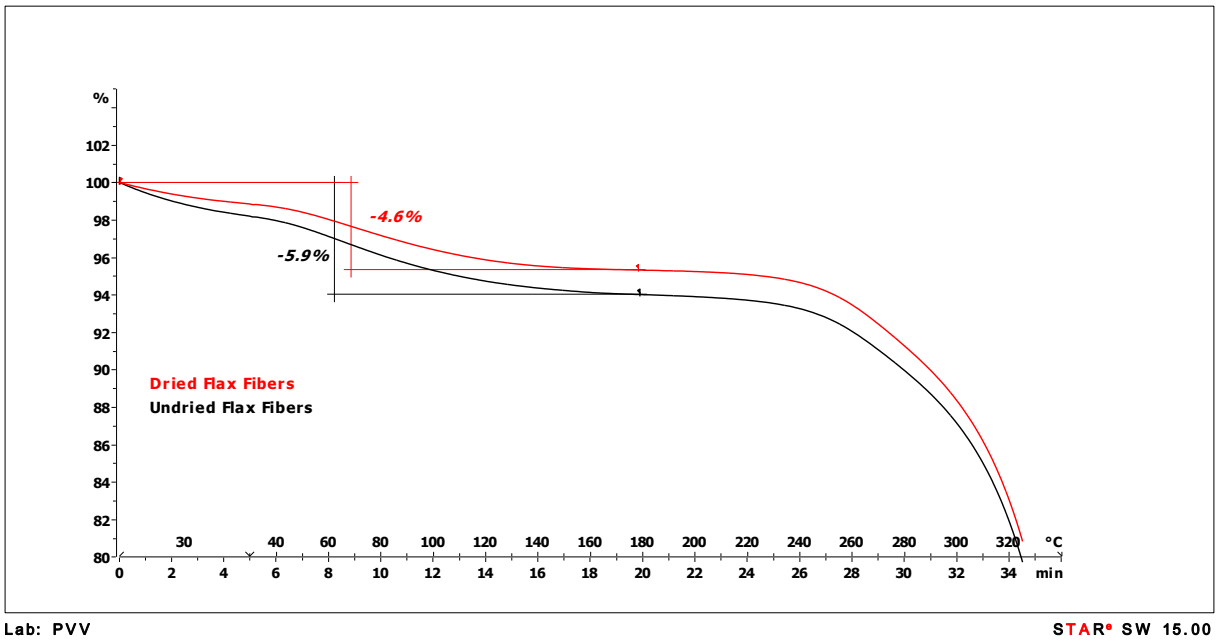

Figure S2

Weight loss of dried and undried flax fibers at 10°C/min under N2 flow after 1 min dwell time at 30°C (instrument : Mettler Toledo, TGA/SDTA851e)